Quantitative Analysis of the Electrostatic Potential in Rock-Salt Crystals Using Accurate Electron Diffraction Data

ARTICLE *in* THE JOURNAL OF PHYSICAL CHEMISTRY B · MAY 2001

Impact Factor: 3.3 · DOI: 10.1021/jp0015729

7 AUTHORS, INCLUDING:

Vladimir G Tsirelson
Mendeleev Russian University of Chemical Te…
172 PUBLICATIONS **1,958** CITATIONS
SEE PROFILE

Ullrich Pietsch
Universität Siegen
411 PUBLICATIONS **3,731** CITATIONS
SEE PROFILE

Quantitative Analysis of the Electrostatic Potential in Rock-Salt Crystals Using Accurate Electron Diffraction Data

V. G. Tsirelson,*,† A. S. Avilov,‡ G. G. Lepeshov,†,‡ A. K. Kulygin,‡ J. Stahn,§ U. Pietsch,§ and J. C. H. Spence||

Department of Quantum Chemistry, Mendeleev University of Chemical Technology, Moscow 125047, Russia, Institute of Crystallography, Russian Academy of Science, Moscow 117333, Russia, Institute of Physics, University of Potsdam, Potsdam D14415, Germany, and Department of Physics and Astronomy, Arizona State University, Tempe, Arizona 85287

Received: April 25, 2000; In Final Form: February 7, 2001

Very accurate electron structure factors measured by a significantly improved transmission electron diffraction technique for polycrystalline samples were used in a high-resolution quantitative study of the electrostatic potentials in LiF, NaF, and MgO crystals. The spatial electrostatic potential distribution was obtained using an analytical structural κ-model adapted for electron diffraction. A topological analysis of the electrostatic potential, defining the features of the electrostatic field and the Coulomb force field in a crystal was developed. In addition to the topological analysis of the electron density, this approach provides a more complete description of the atomic interactions. The application of this approach to the characterization of bonding in a crystal has been demonstrated. The suitability of electron diffraction for determination of the core-electron binding energy is discussed.

Introduction

The electrostatic (Coulomb) inner-crystal potential (EP) is a scalar function

$$\varphi(\mathbf{r}) = \int_{-\infty}^{\infty} \{\sigma(\mathbf{r}')/|\mathbf{r} - \mathbf{r}'|\}\mathrm{d}\mathbf{r}' \quad (1)$$

which depends on the sum of the nuclear and electronic parts of the charge density

$$\sigma(\mathbf{r}') = \sum\nolimits_a Z_a\delta(\mathbf{r}' - \mathbf{R}_a) - \rho(\mathbf{r}') \quad (2)$$

Here Z_a and $\mathbf{R}_a$ are the nuclear charge of atom "a" and nuclear position of atom "a", respectively, $\rho(\mathbf{r}')$ is the electron density (we suppose that $\varphi(\mathbf{r})$ does include the volume average value of the Coulomb potential, which depends on crystal shape and surface structure[1]). The EP distribution reflects the peculiarities of the atomic and molecular interactions as well as the crystal packing features.[2,3] The EP at nuclear positions determines the core-electron binding energy.[4,5] Physical observables may also be calculated from the electrostatic potential (as well as from the electron density) if they take the form of a local one-electron operator.[2,3] The gradient of the electric field at nuclei, important for nuclear quadrupole resonance and Mossbauer spectroscopy, can be obtained from the EP, together with the diamagnetic susceptibility[6] and the refractive index for electrons.[7]

For a given arrangement of nuclei within the unit cell, the correct EP can be obtained from the solution of the corresponding one-electron (Hartree−Fock or Kohn−Sham) equations. On the other hand, a Fourier synthesis of the EP of atoms, molecules, and solids from structure factors can be obtained using high-energy (>10 keV) electron diffraction, because the exchange interaction between the beam electrons and the target electrons at these energies is negligible. The connection between the scattered electron intensities, the electron density, and various components of the molecular potential energy has been established;[8−11] however, only the deformation electron densities[12−16] and electrostatic potentials[17] for some simple molecules have been obtained up to now using gas-phase electron diffraction. The electrostatic potential in solids was studied by electron diffraction as well;[18,19] however, the accuracy of early results was poor.

Recently, as a result of advances in instrumentation (energy filters, CCD detectors, etc.) it has become possible to measure the low-order structure factors of the EP in crystals with very high accuracy by electron microdiffraction.[20−21] This avoids extinction errors since the probe is smaller than a mosaic block, and benefits from the Mott formula relating X-ray and electron structure factors. This formula shows that electron scattered intensity increases as q^{-4} compared to X-ray scattering at the low angles important for bonding. The chemical bond features in copper oxide were recently revealed[22] using this method. We have achieved a similar improvement in the accuracy of structure factors measurement by a factor of 10 for all reflections within the Ewald sphere due to our development of the transmission electron diffraction technique for polycrystalline samples.[23] The opportunity to obtain unusually accurate electron structure factors allowed us to start a high-resolution study of the EP in crystals. We report in this paper the first quantitative results concerned with the EP distribution in LiF, NaF, and MgO crystals obtained using an analytical structural model. A comparison of the experimental EP with the theoretical one, calculated by nonempirical Hartree−Fock methods for a three-dimensional crystal, is also presented.

* Corresponding author. Fax: +7-095-200-4204. E-mail: tsirel@muctr.edu.ru.
† Mendeleev University of Chemical Technology.
‡ Russian Academy of Science.
§ University of Potsdam.
|| Arizona State University.

10.1021/jp0015729 CCC: $20.00
Published on Web 05/04/2001

The presence of accurate experimental data requires the development of more advanced methods of data analysis. Consider the general features of the electrostatic potential. In the stationary state of a system at equilibrium, the EP $\varphi(\mathbf{r}) \rightarrow +\infty$, when $r' \rightarrow \mathbf{R}_a$.[24−25] The behavior of $\varphi(\mathbf{r})$ close to nuclei is, however, indistinguishable from that for a true maxima (the same was noted for the bare nuclear potential[26]). Therefore the nuclear positions can be considered as maxima in $\varphi(\mathbf{r})$. There are no other three-dimensional maxima in the EP;[27] however, two- and one-dimensional maxima do exist. The spatial EP distribution depends on the mutual sizes and charges of the ions. Indeed, the EP of an isolated positive ion and an isolated neutral atom is positive everywhere beyond the nuclear site: it monotonically decays approaching zero with growing $\mathbf{r}$.[28] At the same time, the EP of an isolated mononuclear negative ion monotonically decays, passing through zero and attains a unique negative minimum at some distance from nuclei.[29] When $r \rightarrow \infty$, this EP does approach zero being negative.

The superposition of all ionic contributions defines the features and local sign of the EP in a crystal. The latter depends also on the value of the unit-cell average value of the Coulomb potential φ_0[1], which can be determined experimentally relative to the vacuum level by electron holography[7] or calculated theoretically.[30−31]

Thus, the electrostatic potential of a many-electron many-nuclear system exhibits maxima, saddle points, and minima corresponding to the nuclear positions, internuclear lines, atomic rings, and cages in a crystal unit cell. Therefore, as for the electron density,[2,32−33] the EP can be characterized by critical points (CP), $\mathbf{r}_c$, points at which $\nabla\varphi(\mathbf{r}_c) = 0$. In terms of a topological analysis,[32−33] the critical points corresponding to saddle points, one- and two-dimensional minima in the EP, are denoted as (3,−1) and (3,+1): 3 is the number of nonzero nondegenerated eigenvalues of the Hessian matrix of the EP, λ_i, at $\mathbf{r}_c$, and −1 or +1 is a sum of the algebraic signs of λ_i. Maxima and minima are described by the (3,−3) and (3,+3) CP, correspondingly.

More generally, the EP is characterized by the gradient vector field $\nabla\varphi(\mathbf{r})$, and by the EP curvature, $\nabla^2\varphi(\mathbf{r})$. It is important that all these characteristics do not depend on the constant φ_0, whereas $\varphi(\mathbf{r})$ itself does. The physical meaning of the gradient lines of $\varphi(\mathbf{r})$ is well-known:[34] the classical electrostatic field $\mathbf{E}(\mathbf{r}) = -\nabla\varphi(\mathbf{r})$ is tangential to the gradient lines, the concentration of these lines going through a unit square, perpendicular to them, characterizes the electric field strength at a given point. Gradient lines are not allowed to cross. Pairs of gradient lines in the $\nabla\varphi(\mathbf{r})$ field originated at a (3,−1) CP and terminating at two neighboring nuclei are determined by eigenvectors corresponding to a single positive eigenvalue of the Hessian of the EP at this point, λ_3. They form lines connecting neighboring nuclei, along which the EP is maximal with respect to any lateral shift. The inner-crystal electric field $\mathbf{E}(\mathbf{r})$ exerted on a test (point unit positive) charge along the internuclear line is directed to a (3,−1) CP and changes its direction at this point.

Nuclei of neighboring atoms in any molecule and crystal are separated in the electric field $\mathbf{E}(\mathbf{r})$ by surfaces S_i, satisfying the zero-flux condition

$$\mathbf{E}(\mathbf{r})\cdot\mathbf{n}(\mathbf{r}) = -\nabla\varphi(\mathbf{r})\cdot\mathbf{n}(\mathbf{r}) = 0, \quad \forall\mathbf{r} \in S_i(\mathbf{r}) \qquad (3)$$

where $\mathbf{n}(\mathbf{r})$ is a unit vector normal to the surface. These surfaces define the atomic basins, inside of which the nuclear charge is completely screened by the electronic charge, i.e., electrically neutral *bonded* pseudoatoms. In other words, they define the regions in a crystal dominated by a charge of one or another nucleus.

From the differential form of the Poisson equation $\nabla^2\varphi(\mathbf{r}) = -4\pi\sigma(\mathbf{r})$ and sign-constancy of the electron density follows that $\nabla^2\varphi(\mathbf{r}) = \lambda_1 + \lambda_2 + \lambda_3 > 0$ at every point other than nuclear positions. Because λ_3 is always positive, the restriction $\lambda_1 + \lambda_2 < \lambda_3$ exists.

Thus, the topological features of the electrostatic potential, in addition to those of the electron density,[2,33] carry the physical information on the inner-crystal electrostatic field. The usefulness of the critical point analysis in the study of the EP-dependent properties of molecules was recently noted.[35−36] It would be useful to connect the general pattern of the electrostatic potential, coming from the experiment, with a description of the bonding in a crystal. As a first step, we will present here the results of an analysis of the topological features of the electrostatic potential in LiF, NaF, and MgO.

Experimental Section

Quantitative reconstruction of the EP from electron diffraction data requires as complete as possible a set of structure factors, which have to be known with a statistical precision of 1−2%. To do that we have developed a new precise high-energy transmission electron diffraction device, which measures a diffraction pattern, created by a nearly parallel incident high-stability electron beam passing through a polycrystalline thin film. The construction of the device is described elsewhere.[23] The issues essential for further presentation are as follows.

− A scintillator with 5 ns decay time and a photomultiplier with a time-resolution of 10 ns allow us to register the electrons in an interval of about 15 ns, corresponding to a pulse frequency of 60−70 MHz (a beam current of 10^{-11} A).

− The nonlinearity of the gear frequency characteristics of the registration system does not exceed 0.5% (for frequencies below 1 MHz).

− Computer-controlled, variable two-dimensional step-by-step scanning applied in the accumulation mode provides a statistical precision of intensity measurements of 1%.

− The rather uniform incoherent background is subtracted by assuming a convex spline-fitted connection line between neighboring diffraction maxima in two dimensions. The estimated precision of accounting for the background is better than 0.5%.

The new transmission electron diffraction device was used to measure, at room temperature, the diffraction patterns for polycrystalline films with rock-salt structure with space group $Fm3m$: LiF (parameter of the cubic unit cell $a = 4.024$ Å), NaF ($a = 4.638$ Å), and MgO ($a = 4.212$ Å). An accelerating voltage of 75 keV was applied. Thin films consisting of randomly oriented microcrystallites were prepared in a vacuum (LiF, NaF) and in the air (MgO). During sample preparation, the crystallite sizes were made as small as possible to minimize multi-wave diffraction, responsible for primary extinction. The smoke produced by small crystallites was precipitated on a grid with small cells covered by a thin celluloid film, the grid was rotated around several axes during the process of precipitation to avoid preferential orientation of crystallites. The size of the crystallites obtained was 100−300 Å.

Each diffraction pattern was measured 5 times to provide statistical precision of the intensities to at least 1%. After averaging and background subtraction the merging reflections were separated according to their theoretical values, or with the help of profile analysis (thermal parameters from 19 have been

used). The total number of independent measured reflections was 40 for LiF ($\sin\theta/\lambda = 1.361$ Å^{-1}), 39 for NaF ($\sin\theta/\lambda = 1.38$ Å^{-1}), 40 for MgO ($\sin\theta/\lambda = 1.30$ Å^{-1}).

The experimental intensities were reduced to an absolute scale and used to determine the isotropic thermal parameters of atoms, B, refining the structural model composed by a superposition of spherical atoms. The atomic scattering functions were taken from ref 37. To diminish an effect of atomic asphericity due to chemical bonding, ignored in this model, the refinement was performed over high-angle reflections where the spherical approximation for atomic shapes is valid.[2] The measured B values and corresponding discrepancy factors were obtained as follows: LiF ($\sin\theta/\lambda > 0.61$ Å^{-1}): $B_{Li} = 1.014(9)$, $B_F = 0.901(6)$, $R = 1.32\%$; NaF ($\sin\theta/\lambda > 0.57$ Å^{-1}): $B_{Na} = 0.814(5)$, $B_F = 0.922(5)$, $R = 0.89\%$; MgO ($\sin\theta/\lambda > 0.9$ Å^{-1}): $B_{Mg} = 0.316(4)$, $B_O = 0.342(6)$, $R = 0.70\%$.

The experimental intensities were then analyzed for the presence of extinction. This analysis has shown that the intensities of all reflections in NaF and most of the middle-angle and all high-angle reflections of LiF and MgO are well described within the kinematic theory. Four of the low-angle reflections of LiF and seven of MgO reflections were corrected for primary extinction using the Blackman (two-wave) approximation.[38] Nevertheless, the 400 reflection for LiF and reflections 440 and 444 for MgO have lower intensities even after the correction was applied. We concluded that multiple scattering processes take place in these crystals in certain directions.

Structural κ-Model for Electron Diffraction

The structural model used in the last stage of the refinement was as follows. Replacing $\rho(\mathbf{r})$ in eq 2 by the sum of atomic-like terms $\rho_a\boldsymbol{r}$ over the unit cell ($\rho = \sum_a \rho_a$), one obtains an expression for the EP in the form

$$\varphi(\mathbf{r}) = \sum\nolimits_a \{Z_a/(|\mathbf{r} - \mathbf{R}_a|) - \int_{\infty}^{-\infty} \{\rho_a(\mathbf{r}')/|\mathbf{r} - \mathbf{r}'|\}\mathrm{d}\mathbf{r}'\} \quad (4)$$

Following ref 39, we represent the static electron density ρ_a of the ath pseudoatom by the expression

$$\rho_a(\mathbf{r}) = \rho_{core,\,a}(\mathbf{r}) + P_{val,a}\,\kappa_a{}^3\rho_{val,a}(\kappa_a\mathbf{r}) \quad (5)$$

Here $\rho_{core,a}$ and $\rho_{val,a}$ are spherically averaged free atomic (or ionic) core and valence electron densities normalized to one electron. The κ_a are atomic expansion/contraction parameters and $P_{val,a}$ are atomic electron populations. Fourier transform of eq 4 taking account of eq 5 gives

$$\Phi_a(\mathbf{q}) = (\pi V|\mathbf{q}|^2)^{-1} \sum\nolimits_a \{Z_a - [f_{core,\,a}(\mathbf{q}) + P_{val,a}\, f_{val,a}(\mathbf{q}/\kappa)]\} \quad (6)$$

The structural κ-model, described by the structure factors of eq 6, was fitted to the experimental electron structure factors. We have used the Hartree−Fock single-charged ionic valence and core wave functions[40] to provide the best description of the ions in a crystal. Details of the κ-models refined are specified in Table 1. The thermal atomic motion was described in the harmonic approximation. The thermal parameters were refined using high-angle reflections ($\sin\theta/\lambda \geq 0.7$ Å^{-1}) while κ_a parameters and the atomic electron populations $P_{val,a}$ were refined using low-angle ones. During refinement most of the extinction-affected reflections (400 for LiF and 440 and 444 for MgO) were omitted. The refinement results are listed in Table 1 and Table 2. The quality of fit of the model is illustrated in Figure 1a.

TABLE 1: Results of the Refinement of the Ionic Crystal Structural κ-Models for LiF, NaF, and MgO[a]

		electron diffraction structure amplitudes				Hartree−Fock structure amplitudes		
compound	atom	P_v	κ	R %	R_w %	P_v	κ	R %
LiF	Li	0.06(4)	1[b]	0.99	1.36	0.06(2)	1[b]	0.52
	F	7.94(4)	1[b]			7.94(2)	1.01(1)	
NaF	Na	0.08(4)	1[b]	1.65	2.92	0.10(2)	1[b]	0.20
	F	7.92(4)	1.02(4)			7.90(2)	1.01(1)	
MgO	Mg	0.41(7)	1[b]	1.40	1.66	0.16(6)	1[b]	0.31
	O	7.59(7)	0.960(5)			7.84(6)	0.969(3)	

[a] Structural κ-models were as follows. LiF: $\rho_{cation}(r) = \rho_{1s}(r) + P_{val}\kappa^3\rho_{2s}(\kappa r)$, $\rho_{anion}(r) = \rho_{1s}(r) + P_{val}\kappa^3\rho_{2s,2p}(\kappa r)$; NaF and MgO: $\rho_{cation}(r) = \rho_{1s,2s,2p}(r) + P_{val}\kappa^3\rho_{3s}(\kappa r)$, $\rho_{anion}(r) = \rho_{1s}(r) + P_v\kappa^3\rho_{2s,2p}(\kappa r)$. [b] Parameters were not refined.

TABLE 2: Isotropic Atomic Thermal Parameters, B (Å^2), Obtained with κ-Model

compound	atom	electron diffraction	X-ray diffraction[43]
LiF	Li	1.00(2)	1.050(9)
	F	0.89(1)	0.751(3)
NaF	Na	0.84(2)	0.940(1)
	F	0.93(2)	0.955(2)
MgO	Mg	0.31(2)	0.319(2)
	O	0.34(2)	0.333(3)

Theoretical

To get an estimate of the accuracy of the experimental results, the electron densities of three-dimensional periodic LiF, NaF, and MgO crystals were calculated by the nonempirical Hartree−Fock method for the experimental geometry using the CRYSTAL95 program.[41] The extended 6-11G+, 8-511G, 7-311G*, 8-511G*, and 8-411G* atomic basis sets for Li^+, Na^+, F^-, Mg^{2+}, and O^{2-}, respectively, listed in http://www.dl.ac.uk/TCSC/Software/ CRYSTAL/, were used initially, then optimized to obtain a minimum in crystal energy. The κ-model (eqs 4 and 5) was fitted to the Hartree−Fock structure factors to provide a uniform comparison with experimental results (Table 1). The theoretical electron structure factors were calculated from Fourier transforms of the Hartree−Fock crystal electron density using the Bethe−Mott expression.[38]

A comparison of the model static electron structure factors obtained after a fit of the κ-model to the experimental data and Hartree−Fock calculations is given in Figure 1b. Note, that the accuracy of the structure factors, calculated with the extended basis set close to the Hartree−Fock limit, is, in principle, about 1%.[42]

Electrostatic Potentials

The electrostatic potentials for all crystals were reconstructed from electron diffraction data using static model parameters P_{val} and κ. The calculation of the average inner-cell electrostatic potential with the same parameter,[1−2,30] resulted in the following values of φ_0: 7.07 for LiF, 8.01 for NaF, and 11.47 V for MgO. The latter value may be compared with the electron holography result of 13.01(8) V [7] or with value of 12.64 V obtained for an MgO slab by LAPW calculations.[31] The EP maps in the main planes of the FCC unit cell are presented in Figure 2. In accordance with existing practice[2], these maps are depicted supposing a zero average EP value over the unit cell. The EP for an MgO crystal consisting of point ions with charges ±2e

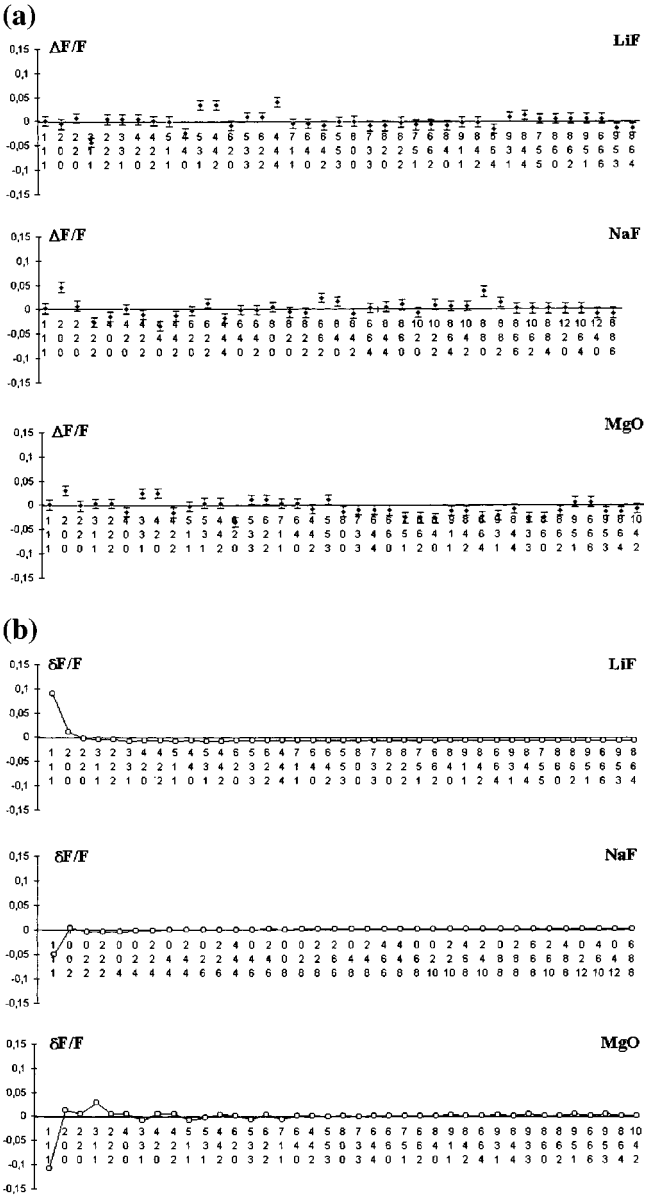

Figure 1. The quality of the fit of κ-model (a) and comparison of the model static structure factors with the Hartree−Fock ones (b). $\Delta F = (F_{exp} - F_{model,\ dyn})/F_{model,\ dyn}$, where F_{exp} and $F_{model,\ dyn}$ are experimental and model dynamic structure factors, while $\delta F = (F_{model,\ stat} - F_{HF})/F_{HF}$, where $F_{model,\ stat}$ are model static and F_{HF} are Hartree−Fock (periodic crystal) static structure factors, correspondingly.

is also shown (Figure 2g,h): it presents the Madelung electrostatic field created by these point charges.

Discussion

The achievement of a precision in electron structure factor measurement of less than 1% has until now only been possible by using the quantitative convergent beam electron diffraction method or the critical voltage method.[20,30] Both these methods deal with single crystals and allow the measurement of low-angle structure factors. The quantitative convergent beam electron diffraction uses an electron probe of nanometer dimensions, so that nanocrystals may be analyzed; however, accuracy for high-order reflections is poorer than the X-ray diffraction provides. The critical voltage method usually gives only a ratio of an unknown to a known reflection. Therefore, these methods are not able to provide a high-resolution reconstruction of the EP without adding X-ray or theoretical structure factors.[21−22] The transmission electron diffraction method for polycrystals is the only one allowing the measurement of all electron structure factors within the Ewald sphere, provided that errors due to multiple scattering are avoided.

Inspection of Figure 1 allows us to conclude that the average uncertainty in the determination of the kinematic experimental electron structure factors in this work can be estimated to be about 1%. Note, that the values of the model structure factors for reflections corresponding to extinction-affected experimental reflections, which were removed during κ-refinement of the LiF and MgO, prove to be in good agreement with the Hartree−Fock ones (Figure 1b).

Comparison of the high-angle electron-diffraction atomic thermal parameters with those obtained by X-ray diffraction [43] (Table 1) shows reasonable agreement with one exception: there is a significant disagreement of B values observed for the F atom in LiF and Na atom in NaF. At the same time, we note considerable disagreement of atomic thermal parameters with those calculated recently using a different approximation.[44] Up to now, we do not have an explanation for this fact, which needs additional study.

The structural κ-model used for the data treatment in this work is the simplest one: it does not describe properly the regions of near-uniform EP, which are restrictively represented in the structure factors. Furthermore, this model, as with any structural crystal model, does not necessarily provide a good partition of the EP distribution for ionic components: only the superposition of mutually penetrating ionic contributions represents the EP. For example, as seen in Figure 1b, a deviation of up to 10% does exist in all crystals for the 111 reflection, which gives a significant contribution to the P_{val} and κ values. Therefore, there is not much sense in discussing the values of P_{val} in Table 1 as estimates for getting the atomic charges. Note that these charges ±0.93e (LiF), ±0.92e (NaF), and ±1.59e (MgO) reflect the interionic charge transfers in correspondence with the accepted representation of an ionic bond in rock-salt crystals. At the same time, they differ from the formal oxidation numbers assigned to ions in these compounds.

The calculation of the electrostatic potential from electron structure amplitudes was done by Fourier method at an early stage.[2,18−19] Independently of the experimental precision achieved, the corresponding (dynamic) EP maps suffered from Fourier series cutoff due to an insufficient number of measured Fourier coefficients: false minima and maxima of about 50 V are observed around atomic positions at a resolution of ∼0.3 Å.[19] Therefore, Fourier maps can be considered as qualitative only. In addition, the Fourier-reconstructed EP distribution consists of the contributions from all electrons and nuclei of the crystal, and therefore contains the "self-interaction potential".[34,45] That EP will result in an unphysical electrostatic energy (energy of the electrostatic interactions of the nuclei and electrons per unit cell) containing the self-interaction energy terms.

The calculation of the EP with a proper analytical model is free from Fourier series termination effects and allows easy accounting for the nuclear self-potential. In our experimental situation, the nuclei are considered as point charges, and the self-potential correction for nuclear position $\mathbf{R}_a$ is achieved by removing the contribution of nuclear charge Z_a in eq 4. The corresponding correction for each point of the electron density is negligible because an infinitely small element of the electronic charge should be removed. The self-corrected EP values at the nuclear positions in the studied crystals, derived from the electron diffraction and Hartree−Fock data with the κ-model,

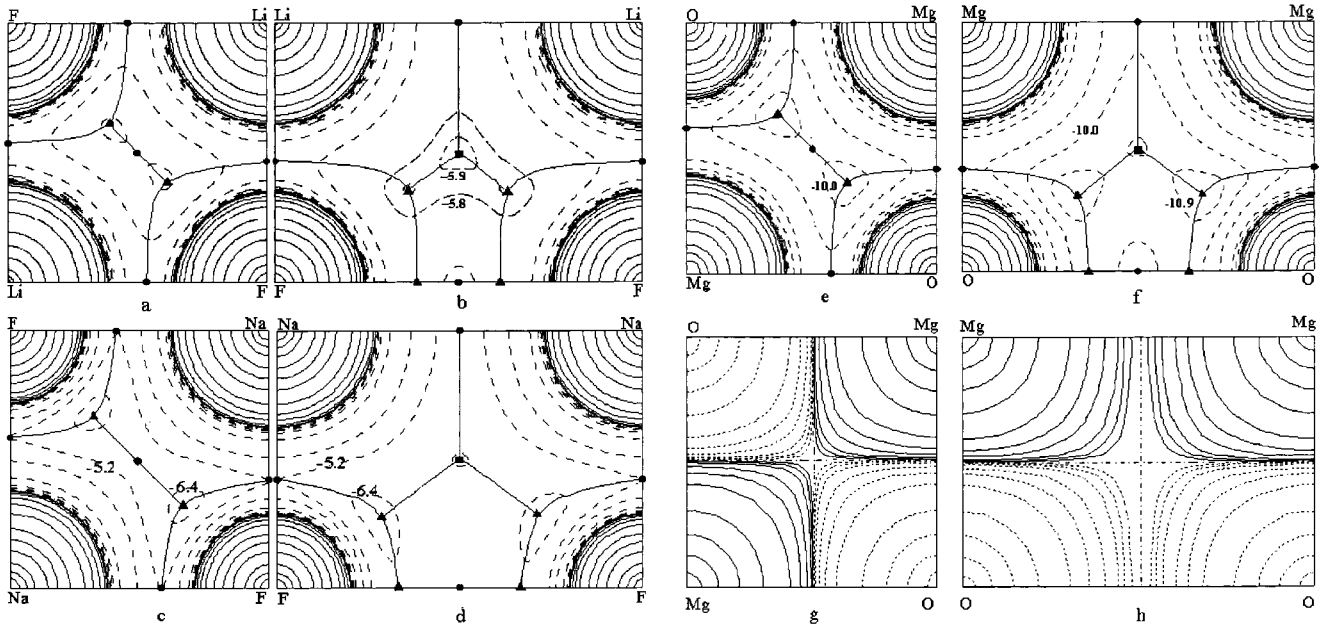

Figure 2. Experimental (model static) electrostatic potential distributions overlaid with zero-flux interatomic surfaces in the $\nabla\varphi(\mathbf{r})$ field in (100) and (110) planes of the cubic unit cell of LiF (a,b), NaF (c,d), and MgO (e,f). Critical points (3,−1), (3,+1), and (3,+3) in the electrostatic potential are denoted by the dots, triangles, and squares, correspondingly. The electrostatic potential for MgO crystal consisting of point ions with charges ±2e is also shown (g,h). Solid and dashed lines correspond to the positive and negative values of the potential, correspondingly, dot−dashed lines represent the zero potential value. Contours are 0, ±0.2, ±0.4, ±0.8, ±2, ±4, ±8, ... V. Some additional contours are specified in the maps. Electrostatic potential in Figure 2g,h was chosen as zero at the center on the Mg−O bond.

TABLE 3: Values of the Electrostatic Potentials (V) at the Nuclear Positions in Crystals and Free Atoms

			Hartree−Fock (crystal)		
		electron diffraction (κ-model)	direct space[48]	reciprocal space (κ-model)	atoms[25]
LiF	Li	−158(2)	−159.6	−158.1	−155.6
	F	−725(2)	−726.1	−727.2	−721.6
NaF	Na	−968(3)	−967.5	−967.4	−964.3
	F	−731(2)	−726.8	−727.0	−721.6
MgO	Mg	−1089(3)	−1090.5	−1088.7	−1086.7
	O	−609(2)	−612.2	−615.9	−605.7

TABLE 4: "Bonded Radii" Derived from the Electrostatic Potential and Electron Density[a]

		"bonded radii" (Å)	
compound	atom	electrostatic potential	electron density
LiF	Li	1.084	0.779
	F	0.928	1.233
NaF	Na	1.355	1.064
	F	0.964	1.255
MgO	Mg	1.207	0.918
	O	0.899	1.188

[a] "Bonded ionic radius" is defined as a distance from a nuclear position to the one-dimensional minimum in the electrostatic potential or electron density along the bond direction.

are presented in the Table 3. Nuclear charge Z_a does not contribute to the EP when $\mathbf{r}' = \mathbf{R}_a$ and the EP in this point is determined by the electron density contribution because the influence of other nuclei is negligibly small. Inspection of this table shows that experimental EP values are close to the ab initio calculated ones, both differing in crystals from their free atom analogues.[25] It was shown [4,5] that this difference in the electrostatic potential at nuclear positions correlates well with the 1s-electron binding energy. Therefore, the electron diffraction data carry, in principle, information about bonding in a crystal which is usually obtaining by photoelectron spectroscopy.[4] We conclude that the suitability of electron diffraction for the quantitative determination of core-electron binding energy deserves special analysis.

Consider now the EP distributions in the main planes of the FCC cubic unit cell (Figure 2). The EP along the cation−anion line in all the crystals studied has a smooth character with a single axial one-dimensional minimum at a distance of 0.928, 0.964, and 0.899 Å from the anion site in LiF, NaF, and MgO, correspondingly (Table 4). The location of this minimum reflects the difference in the EP distribution of ions and depends on the crystal structure. Compare LiF and NaF, for example. The negative EP minima of single (removed from a crystal) F ions with P_v and κ as those from electron diffraction experiments for LiF and NaF (see Table 1) are located at a distance of 1.06 and 1.03 Å from the nuclei, correspondingly. The positive EP of the relatively larger Na ion diminishes more slowly than the EP of Li; however, the unit cell parameter in NaF is larger. As a result, the distances of the axial minimum positions from anions in LiF and NaF crystals are very close to each other.

One-dimensional maxima in the EP are observed in the center of the anion−anion line in the (100) plane: they join smoothly the pair of two-dimensional minima lying on the same line close to anion positions. These minima explicitly reflect the acquisition of excess electronic charge by F atoms in a crystal, and their existence is a consequence of the specific **r**-dependence of the EP of negatively charged atoms as discussed in the Introduction. Analysis shows that the more the negative charge of any single ion increases, the more the corresponding negative EP minimum value is lowered; simultaneously the position of this minimum is slightly shifted to the nucleus. The κ parameter only slightly influences the minimum characteristics. In a crystal, this feature distinctively manifests itself as the areas of the minimal EP far from the nearest-bond lines, where cation contributions to the EP do not dominate. Similar minima in the electrostatic potential were recently found around F atoms in

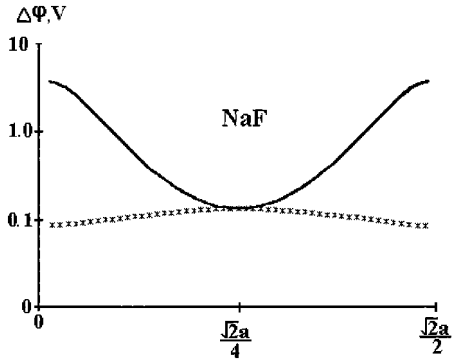

Figure 3. Difference between experimental (model static) and Hartree−Fock (three-dimensional periodic calculation) electrostatic potentials along the Na−Na (solid lines) and F−F ("star" lines) directions in the (100) plane of the cubic unit cell of NaF.

$KNiF_3$ [46] and O atoms in $KTaO_3$ and $SrTiO_3$,[47] as well as close to the negatively charged atoms far from the bond lines in heteroatomic molecules.[35−36] Thus, the appearance of minima in the electrostatic potential in "non-bonded" directions is a very sensitive indicator of the presence of interatomic charge transfer in a crystal (and in molecules). Note, that the sign of the EP in these minima does depend on the choice of the EP zero, and hence on the mean value of the electrostatic potential.

To check the reliability of our results we have computed the difference between experimental (static model) and Hartree−Fock (CRYSTAL95 calculation) electrostatic potentials. Figure 3 demonstrates this difference for NaF: the discrepancy for other crystals has an even lower value.

Thus, the EP features described are reproduced both in the electron diffraction and the Hartree−Fock calculations, including the position space analysis in the latter case.[48] The same features were also found in the treatment of the X-ray diffraction data within the more flexible multipole model instead of the κ-model.[49] Therefore, it can be concluded that the presence of these features in the EP potential is not an artifact.

Using the critical point terminology, we can say that the (3,−1) CPs in the EP situate at the cation−anion and cation−cation lines (Figure 2). They are characterized by two negative curvatures of the EP along directions perpendicular to these lines and one positive curvature along them. The two-dimensional minima found on the anion−anion line in the (100) plane correspond with the (3,+1) CPs in the three-dimensional EP distribution. The (3,+3) CPs are observed at the centers of the cubes formed by four cations and four anions.

Comparing the critical point patterns in the electron density (Figure 4) and electrostatic potential (Figure 2e) in MgO, which gives a typical example, we note that the CP arrangements do not coincide. It was shown [26] that the bare nuclear potential also gives a critical point pattern different from those of the electron density. These observations are manifestations of the well-known fact that the electron density (and energy) of a many-electron system is not determined entirely by the nuclear and electron Coulomb electric field.

The EP defining the inner-crystal electrostatic field created by all nuclei and electrons at point $\mathbf{r}$, $\mathbf{E}(\mathbf{r}) = -\nabla\varphi(\mathbf{r})$, defines also the value of the classical electrostatic (one-electron) Coulomb force acting at $\mathbf{r}$. The CPs in the EP are points where the electric field $\mathbf{E}(\mathbf{r})$ vanishes. Correspondingly, they are points where the inner-crystal Coulomb force is zero. At the nuclear positions, this is in agreement with the requirements of the Hellmann−Feynman theorem [50] applied to a system at equilibrium. We also note that there are points in the internuclear

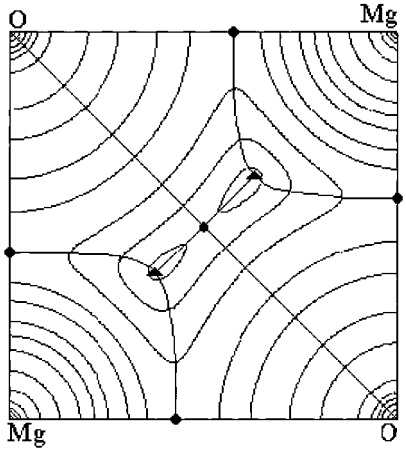

Figure 4. Electron density distribution in the (100) plane of MgO calculated with parameters of κ-model fitted to the electron diffraction structure amplitudes. Contours are 0.2, 0.4, 0.8, 2, 4, 8, ... e Å^{-3}. Critical points (3,−1) and (3,+1) are denoted by the dots and triangles, correspondingly. Zero-flux interatomic surfaces in the $\nabla\rho$ ($\mathbf{r}$) field and O−O interaction line are shown as well.

space where the Coulomb force acting on an element of the electron density is zero. Recalling the expression for the electrostatic energy density[34] $w(\mathbf{r}) = (1/8\pi)\,[\mathbf{E}(\mathbf{r})]^2$, we can see that this value is zero at the critical points as well.

For the crystals under examination, the zero-flux atomic surfaces in the $\nabla\varphi(\mathbf{r})$ field, defined by eq3, are showed in Figure 2. Zero-flux atomic surfaces naturally partition the electrostatic potential in a crystal into the atomic-like nucleus-charge-dominated regions. Each element of the electron density within these regions will be attracted by corresponding nuclei. Therefore, the shape and size of these regions reflect the electrostatic balance between electrons and nuclei of bonded atoms in a crystal (ions), not the sizes of the ions in a crystal governed by quantum mechanics[33] (Figure 4). That is why the positions of the EP minima on the bond lines cannot be used for the estimation of the radii of ions: the electron density is much more suitable for this purpose[33] (see Table 4). A comparison of the shapes of the zero-flux regions in the EP with those in the electron density makes clearer the role of different factors in the crystal structure formation. For example, the manifestation of the quantum effects during the rock-salt-type crystal formation consists of diminishing the size of the cations and extending the atomic basin of anions accompanied with formation of the anion−anion interaction in the (001) plane (Figure 4). Analogous analysis for perovskites, which has been also done recently,[51] resulted in the same conclusions.

The lines formed by pairs of electric field gradient lines terminating at the (3,−1) critical points in the EP correspond to the nearest cation−anion and cation−cation distances in a crystal with the rock-salt structure. Because of the correspondence between interacting charges and their electric fields, these lines can be considered as images of the electrostatic atomic interactions. In the perovskites, the (3,−1) critical points in the EP were found on the following lines: Ni−F, K−F, Ni−K, K−K in $KNiF_3$,[46] Ti−O, Sr−O, Ti−Sr, Sr−Sr in $SrTiO_3$, and Ta−O, K−O, Ta−K, K−K in $KTaO_3$.[47] These observations do not match the pattern of the pairwise Coulomb interactions between *all* ions used normally in calculations of the electrostatic energy of a crystal:[2,52] no lines connecting the anions were found in the $\nabla\varphi(\mathbf{r})$ field (no such atomic interaction lines are found in perovskites[46,47,53] as well). As follows from this gradient field consideration, the Coulomb interactions are transmitted through

a crystal in the form of the "atom−atom interactions", a network of which is a specific property of each compound (or of each crystal structural type).

The crystal electric field pattern resulting from the experimental EP differs strongly from that created by an infinite array of positive and negative point charges placed at the atomic positions in a crystal (Figure 2g,h). It was pointed out[54] (see also Figure 2), that the latter (Madelung) field of a crystal is partitioned by zero-flux boundaries into bond-like regions instead of atomic-like ones. According to ref 54, each bond-localized region can be characterized by the point-charge electric field flux linking the nearest-neighboring cations and anions. This flux was identified with bond valence, and a correspondence obtained between Gauss' law and the valence-sum rule of the empirical bond-valence model.[55] We should keep in mind however, that any system of static interacting point charges cannot be stable (Earnshaw theorem[34]). Moreover, it is impossible to describe bonding in such a system.[56] Therefore, physically reasonable considerations of the Coulomb field features in a crystal have to take into account the whole EP distribution.

It is worth noting that even bond-like Madelung field partitioning does not match the appearance of the overall pairwise Coulomb interactions between "point" ions, because only nearest-neighbor bonding contacts are taking into account in the ionic model.[54]

Acknowledgment. The Authors thank Professor I. D. Brown for valuable discussions. The work was supported by the Deutsche Forschungsgemeinschaft (Grant Pi217/13-2), U.S. Civilian Research and Development Foundation (Grant RP1-208), NSF Award DMR9814055, and Russian Foundation for Basic Research (Grant 98-03-32654).

References and Notes

(1) O'Keeffe, M. A.; Spence, J. C. H. *Acta Crystallogr.* **1993**, *A50*, 33.
(2) Tsirelson V. G.; Ozerov R. P. *Electron Density and Bonding in Crystals: Theory and Diffraction Experiments in Solid State Physics and Chemistry;* Inst. Physics Publ.: Bristol, Philadelphia, 1996.
(3) Molecular Electrostatic Potentials. In *Concepts and Applications*; Murray, J. S., Sen, K., Eds.; Elsevier: Amsterdam, 1996.
(4) Basch, H. *Chem. Phys. Lett.* **1970**, *6*, 337.
(5) Schwarz, M. E. *Chem. Phys. Lett.* **1970**, *6*, 631.
(6) Ramsey, N. F. *Phys. Rev.* **1950**, *78*, 699.
(7) Gajdardziska-Josifovska, M.; McCartney, M.; Weiss, J. K.; De Ruijter, W.; Smith, D. J.; Zuo, J. M. *Ultramicroscopy* **1993**, *50*, 285.
(8) Tavard, C.; Roux, M. *Compt. Rend.* **1965**, *260*, 4933.
(9) Bartell, L. S.; Gavin, R. M. *J. Am. Chem. Soc.* **1964**, *86*, 3493.
(10) Bonham, R. A. *J. Chem. Phys.* **1967**, *71*, 856.
(11) Bonham, R. A.; Fink, M.; Kohl, D. A.; Peixoto, E. M. *Int. J. Quantum Chem.* **1970**, *3S*, 447.
(12) Kohl, D. A.; Bartell, L. S. *J. Chem. Phys.* **1969**, *51*, 2896.
(13) Kohl, D. A.; Bartell, L. S. *J. Chem. Phys.* **1969**, *51*, 2905.
(14) Fink, M.; Moore, P. G.; Gregory, D. *J. Chem. Phys.* **1979**, *71*, 5227.
(15) Fink, M.; Schmiedekamp, C. W.; Gregory, D. *J. Chem. Phys.* **1979**, *71*, 5238.
(16) Fink, M.; Schmiedekamp, C. W.; Gregory, D. *J. Chem. Phys.* **1979**, *71*, 5243.
(17) Fink, M.; Bonham, R. A. In *Chemical Applications of Atomic and Molecular Electrostatic Potentials*; Politzer, P., Truhlar, D. G., Eds.; Plenum Press: New York, 1981; p 93.
(18) Vainshtein, B. K. *Quart. Rep.* **1960**, *14*, 105.
(19) Tsirelson, V. G.; Avilov, A. S.; Abramov, Yu. A.; Belokoneva, E. L.; Kitaneh, R.; Feil, D. *Acta Crystallogr.* **1998**, *B54*, 8.
(20) Spence, J. C. H.; Zuo, J. M. *Electron Microdiffraction*; Plenum Press: New York, 1992.
(21) Zuo, J. M.; O'Keeffe; M. O.; Rez, P.; Spence, J. C. H. *Phys. Rev. Lett.* **1997**, *78*, 4777.
(22) Zuo, J. M.; Kim, M. Y.; O'Keeffe, M.; Spence, J. C. H. *Nature* **1999**, *401*, 49.
(23) Avilov, A. S.; Kulygin, A. K.; Pietsch, U.; Spence, J. C. H.; Tsirelson, V. G.; Zuo, J. M. *J. Appl. Crystallogr.* **1999**, *32*, 1033.
(24) Politzer, P. *Isr. J. Chem.* **1980**, *19*, 224.
(25) Wang, J.; Smith, V. H. *Mol. Phys.* **1997**, *90*, 1027.
(26) Tal, Y.; Bader, R. F. W.; Erkku, R. *Phys. Rev.* **1980**, *A21*, 1.
(27) Pathak, R. K.; Gadre, S. R. *J. Chem. Phys.* **1990**, *93*, 1770.
(28) Weinstein, H.; Politzer, P.; Srebrenik, S. *Theor. Chim. Acta* **1975**, *38*, 159.
(29) Sen, K. D.; Politzer, P. *J. Chem. Phys.* **1989**, *90*, 4370.
(30) Spence, J. C. H. *Acta Crystallogr.* **1993**, *A49*, 231.
(31) Kim, M. Y.; Zuo, J. M.; Spence, J. C. H. *Phys. Stat. Solidi (a)* **1998**, *166*, 455.
(32) Morse, M.; Cairns, S. S. *Critical Point Theory in Global Analysis and Differential Geometry*; Academic Press: New York, 1969.
(33) Bader, R. F. W. *Atoms in Molecules−A Quantum Theory*; Oxford University Press: Oxford, 1990.
(34) Tamm, I. E. *Fundamentals of the Theory of Electricity*; Mir Publ.: Moscow, 1979.
(35) Koester, A. M.; Lebouf, M.; Salahub, D. R. In *Molecular Electrostatic Potentials. Concepts and Applications*; Murray, J. S., Sen, K., Eds.; Elsevier: Amsterdam, 1996; p 105.
(36) Gadre, S. R.; Bhadane, P. K.; Pundlik, S. S.; Pingale, S. S. In *Molecular Electrostatic Potentials. Concepts and Applications*; Eds.; Murray, J. S., Sen, K., Eds.; Elsevier: Amsterdam, 1996; p 219.
(37) *International Tables for Crystallography*, v. C; Wilson, A. J. C., Ed.; Kluwer Academic Publishers: Dordrecht, 1995.
(38) Cowley, J. M. *Diffraction Physics*, Sec. Rev. ed.; North-Holland Personal Library. Elsevier: Amsterdam, 1990.
(39) Coppens, P.; Guru Row, T. N.; Leung, P.; Stevens, E. D.; Becker, P.; Yang, Y. W. *Acta Crystallogr.* **1979**, *A35*, 63.
(40) Clementi, E.; Roetti, C. *At. Data Nucl. Data Tables* **1974**, *14*, 177.
(41) Dovesi, R.; Saunders: V. R.; Roetti, C.; Causa, M.; Harrison, N. M.; Orlando, R.; Aprà, R. *CRYSTAL95, User's Manual*; University of Torino: Torino, 1996.
(42) Weiss, R. J. *X-ray Determination of the Electron Distribution*. Amsterdam: North-Holland, 1966.
(43) Tsirelson, V. G.; Abramov, Yu. A.; Zavodnik, V. E.; Stash, A. I.; Belokoneva, E. L.; Stahn, J.; Pietsch, U.; Feil, D. *Struct. Chem.* **1998**, *9*, 249−254.
(44) Gao, H. X.;, Peng, L.-M.; Zuo, J. M. *Acta Crystallogr.* **1999**, *A55*, 1014.
(45) Bertaut, E. F. *J. Phys. Chem. Solids* **1978**, *39*, 97.
(46) Tsirelson, V.; Ivanov, Yu.; Zhurova, E.; Zhurov, V.; Tanaka, K. *Acta Crystallogr.* **2000**, *B56*, 197.
(47) Zhurova, E. Sagamore XII. Conference on Charge, Spin and Momentum densities. *Book of Abstracts* **2000**, 43.
(48) Stahn, J.; Tsirelson. V. G. Unpublished results, 1997.
(49) Avilov, A.; Lepeshov, G.; Kulygin, A.; Zavodnik, V.; Belokoneva, E.; Tsirelson, V.; Stahn, J.; Pietsch, U.; Spence, J. Eighteenth European Crystallographic Meeting. Abstracts. Praha, August, 15−20. **1998**, p 46.
(50) Feynman, R. P. *Phys. Rev.* **1939**, 56, 340; Hellmann, H. *Einfuerung in die Quantum-chemie*; Deuticke: Leipzig, 1937.
(51) Zhurova, E. A.; Tsirelson, V. G. *J. Phys. Chem. Solids.* Accepted for publication.
(52) *Computer Modelling in Inorganic Crystallography*; Catlow, C. R. A., Ed.; Academic Press: San Diego, 1997.
(53) Luana, V.; Costales, A.; Martin Pendas, A. *Phys. Rev.* **1997,** 55, 4285.
(54) Preiser, C.; Loesel, J.; Brown, I. D.; Kunz, M.; Skowron, A. *Acta Crystallogr.* **1999**, *B55*, 698.
(55) Brown, I. D. *Acta Crystallogr.* **1992**, *B48*, 553.
(56) Teller, E. *Rev. Mod. Phys.* **1962**, *34*, 627; Balasz, N. L. *Phys. Rev.* **1967**, *156*, 42.